HHS Public Access

Author manuscript

Science. Author manuscript; available in PMC 2018 January 06.

Published in final edited form as:

Science. 2017 January 06; 355(6320): 78–83. doi:10.1126/science.aah4199.

Rb1 and *Trp53* cooperate to suppress prostate cancer lineage plasticity, metastasis, and antiandrogen resistance

Sheng Yu Ku[1,*], **Spencer Rosario**[1,*], **Yanqing Wang**[1], **Ping Mu**[2], **Mukund Seshadri**[1], **Zachary W. Goodrich**[1], **Maxwell M. Goodrich**[1], **David P. Labbé**[3,4], **Eduardo Cortes Gomez**[5], **Jianmin Wang**[5], **Henry W. Long**[3,4], **Bo Xu**[6], **Myles Brown**[3,4], **Massimo Loda**[4,7,8,9], **Charles L. Sawyers**[2,10], **Leigh Ellis**[1,†], and **David W. Goodrich**[1,†]

[1]Department of Pharmacology and Therapeutics, Roswell Park Cancer Institute (RPCI), Buffalo, NY 14263, USA

[2]Human Oncology and Pathogenesis Program, Memorial Sloan Kettering Cancer Center (MSKCC), New York, NY 10065, USA

[3]Center for Functional Cancer Epigenetics, Dana-Farber Cancer Institute, Boston, MA 02115, USA

[4]Department of Medical Oncology, Dana-Farber Cancer Institute, Boston, MA 02115, USA

[5]Department of Biostatistics and Bioinformatics, RPCI, Buffalo, NY 14263, USA

[6]Department of Pathology, RPCI, Buffalo, NY 14263, USA

[7]Department of Medical Oncology, Center for Molecular Oncologic Pathology, Dana-Farber Cancer Institute and Brigham and Women's Hospital, Harvard Medical School, MA 02115, USA

[8]Department of Pathology, Brigham and Women's Hospital, Harvard Medical School, MA 02115, USA

[9]Division of Cancer Studies, King's College London, London SE1 9RT, UK

[10]Howard Hughes Medical Institute, Chevy Chase, MD 20815, USA

Abstract

Prostate cancer relapsing from antiandrogen therapies can exhibit variant histology with altered lineage marker expression, suggesting that lineage plasticity facilitates therapeutic resistance. The mechanisms underlying prostate cancer lineage plasticity are incompletely understood. Studying mouse models, we demonstrate that *Rb1* loss facilitates lineage plasticity and metastasis of prostate adenocarcinoma initiated by *Pten* mutation. Additional loss of *Trp53* causes resistance to antiandrogen therapy. Gene expression profiling indicates that mouse tumors resemble human

†Corresponding author. david.goodrich@roswellpark.org (D.W.G.); leigh.ellis@roswellpark.org (L.E.).
*These authors contributed equally to this work.

SUPPLEMENTARY MATERIALS
www.sciencemag.org/content/355/6320/78/suppl/DC1
Materials and Methods
Figs. S1 to S9
Tables S1 and S2
Reference (30)

prostate cancer neuroendocrine variants; both mouse and human tumors exhibit increased expression of epigenetic reprogramming factors such as Ezh2 and Sox2. Clinically relevant Ezh2 inhibitors restore androgen receptor expression and sensitivity to antiandrogen therapy. These findings uncover genetic mutations that enable prostate cancer progression; identify mouse models for studying prostate cancer lineage plasticity; and suggest an epigenetic approach for extending clinical responses to antiandrogen therapy.

As molecularly targeted cancer therapy improves, lineage plasticity is increasingly appreciated as a potential mechanism underlying therapeutic resistance. Lineage plasticity facilitates conversion of a cancer cell that is dependent on the therapeutic target to one that is indifferent to its function. For example, relapse of *EGFR* (epidermal growth factor receptor) mutant lung adenocarcinomas after EGFR-targeted therapy is associated with the appearance of histologically distinct variants that lack *EGFR* expression but express neuroendocrine lineage markers such as *SYP* (1, 2). Likewise, prostate adenocarcinoma (PADC) relapsing from antiandrogen therapies (ADTs) is associated with histological variants exhibiting altered histology, reduced androgen receptor (AR) levels, and expression of neuroendocrine markers (3–5). These neuroendocrine prostate cancer variants (NEPCs) emerge from PADC because they share clonal origin (5–8). The identification of effective therapies for NEPCs has been hindered by incomplete understanding of the mechanisms driving lineage plasticity and the lack of relevant experimental models.

The retinoblastoma tumor suppressor gene *RB1* is more commonly mutated in metastatic and ADT-recurrent prostate cancer—NEPC variants in particular—than it is in primary tumors (5, 9–12). This suggests that there is selective pressure for RB1 loss during tumor evolution and that loss of this gene might drive PADC progression and lineage plasticity. To test this hypothesis, we engineered *Rb1* deletion in a previously characterized mouse model of PADC initiated by *Pten* mutation (13). In the original model, the PBCre4 transgene (14) is used to delete floxed *Pten* alleles specifically in prostate epithelium (fig. S1). PBCre4:$Pten^{f/f}$ mice, where *f* designates a floxed allele, develop prostatic intraepithelial neoplasia (PIN) by 6 weeks of age and invasive PADC by 9 weeks, but these cancers rarely progress to metastatic disease (13, 15–17). Prostate cancer in PBCre4:$Pten^{f/f}$:$Rb1^{f/+}$ mice is similar, so both genotypes are used interchangeably here and are referred to as single knockout (SKO). *Rb1* mutation alone is insufficient to initiate prostate cancer development in the mouse because PBCre4:$Rb1^{f/f}$ mice do not develop prostate cancer (18, 19). The combination of these mutations in PBCre4:$Pten^{f/f}$:$Rb1^{f/f}$ (DKO) mice leads to prostate cancer development, and the mice had a significantly shorter median survival of 38 weeks compared with 48 weeks for SKO mice (Fig. 1A). *Rb1* loss did not affect end-stage tumor cell proliferation significantly, but similar to the loss of the tumor suppressor gene *Trp53* (17), *Rb1* loss abrogated the cellular senescence that occurs in *Pten*-deficient, premalignant prostate epithelium (fig. S2).

End-stage SKO PADC showed expression of phosphorylated AKT (pAKT), nuclear AR, and the luminal epithelial marker Krt8 (Fig. 1B). Expression of the basal epithelial marker Trp63 was low, and expression of the neuroendocrine marker Syp was undetectable. DKO PADC also showed expression of pAKT, but Krt8 and AR levels were heterogeneous between cells

and regionally within contiguous tumors (Fig. 1B and fig. S3A). DKO PADCs also contained cells expressing Syp. Cells surrounding acini were Krt8^{high}:Syp^{low}, whereas cells interspersed between acini were Krt8^{low}:Syp^{high} (fig. S3B), suggesting the presence of at least two molecularly distinct cell populations within these tumors.

Metastasis was not detected in SKO mice, which is consistent with previous reports (15–17). In contrast, distant metastasis was detected in all DKO mice examined to date (Fig. 1C). Common metastatic sites were lymph node, lung, and liver. Bone metastasis was detected in 2 of 10 mice; this is likely an underestimate because we examined only a tibia and femur. All metastases recapitulated the heterogeneous Syp and Krt8 expression pattern of the primary tumors. Metastases disseminated through the vasculature because DKO cancer cells marked by green fluorescent protein (GFP) in PBCre4:*Pten*$^{f/f}$:*Rb1*$^{f/f}$:*Rosa*$^{mT/mG}$ mice (20) were detected in both peripheral blood and bone marrow (Fig. 1, D and E). These observations suggest that *Rb1* suppresses metastatic dissemination of PADC initiated by *Pten* loss.

The existence of both luminal-like Krt8^{high}: Syp^{low} cells and neuroendocrine-like Krt8^{low}: Syp^{high} cells within DKO primary and metastatic tumors suggests that these cancers exhibit lineage plasticity, but other explanations are possible. To explore whether molecular heterogeneity is a consequence of polyclonal tumors, we incorporated the Brainbow 2.1 lineage tracing allele (21) into DKO mice. All end-stage tumors were monocolor, with one and sometimes two independent primary tumors per mouse (fig. S3C). Thus, DKO tumors, both primary and metastatic, were likely derived from a single neoplastic cell clone. Mosaic Cre-mediated gene deletion within tumor clones may also contribute to molecular heterogeneity. RNA-sequencing (RNA-seq) analysis of tumor specimens revealed a few reads mapping to Cre-deleted exons (fig. S3D); these reads are likely contributed by non-epithelial cells that contaminate the bulk tumor specimens. Immunostaining of tumor tissue sections also failed to detect cells expressing protein encoded by the deleted gene (fig. S3E). Thus, it is unlikely that mosaic Cre deletion accounts for the molecular heterogeneity observed.

To characterize the origin of Syp^{high} cells, we performed a longitudinal study of DKO PADC development. PIN lesions and early invasive PADC were apparent in DKO mice by 12 weeks of age, but these neoplastic lesions lacked Syp^{high} cells (fig. S3F). Small foci of Syp^{high} cells were readily detectable by 20 to 25 weeks of age. These early Syp^{high} foci are Krt8^{low} but still express AR (fig. S3G). These observations are consistent with the derivation of Krt8^{low}:Syp^{high} cells from preexisting Krt8^{high}:Syp^{low} neoplasia. We cannot, however, exclude the possibility that Krt8^{low}:Syp^{high} cells arise independently, perhaps from a different cell type of origin, and they subsequently give rise to Krt8^{high}:Syp^{low} cells in tumors. Either scenario is consistent with the hypothesis that *Rb1* loss enhances lineage plasticity of prostate neoplasia initiated by *Pten* loss.

Previous work has shown that PBCre4:*Rb1*$^{f/f}$*: Trp53*$^{f/f}$ mice develop AR^{low}, castration-resistant, NEPC-like tumors exclusively from within the stem cell–rich proximal region of the prostate (18, 22). DKO tumors, in contrast, appeared in the anatomically distinct distal region of the prostate (fig. S4A). Whereas DKO PIN lesions were detected within the

proximal prostate, they exhibited an AR^{high}:Syp^{low} phenotype; in contrast, the earliest PIN lesions detected in PBCre4:*Rb1*$^{f/f}$:*Trp53*$^{f/f}$ mice were AR^{low}:Syp^{high} (fig. S4B). The AR and Krt8 immunostaining patterns were different in DKO and PBCre4:*Rb1*$^{f/f}$: *Trp53*$^{f/f}$ tumors (fig. S4C). These observations suggest that the cell of origin is different in DKO and PBCre4:*Rb1*$^{f/f}$:*Trp53*$^{f/f}$ prostate cancers.

PBCre4:*Rb1*$^{f/f}$:*Trp53*$^{f/f}$ tumors are ADT-resistant de novo because castration does not extend survival (18). However, the AR levels in DKO tumors are higher (fig. S4D), suggesting that they may be ADT sensitive. To test this, we surgically castrated 30-week-old, tumor-bearing DKO mice and monitored their survival. Castration extended median survival of DKO mice from 38 to 48 weeks (Fig. 2A), but all mice eventually died from prostate cancer by 67 weeks. The response of individual mice varied considerably, with postcastration survival ranging from 3 to 37 weeks, but survival did not correlate consistently with precastration total prostate volume (Fig. 2, B and C). DKO cancer that relapsed after castration retained heterogeneous Krt8 and Syp expression but showed markedly reduced AR levels (Fig. 2D). Bone metastasis was detected in three of eight mice with postcastration recurrent disease. We found that two of five postcastration recurrent cancers analyzed with RNA-seq had acquired spontaneous *Trp53* mutations (Fig. 2E). The *Trp53* mutations are analogous to loss-of-function R282Q and V173M mutants found commonly in human cancers. *Trp53* mutations were not detected in eight DKO tumors from noncastrated mice. This implies that *Trp53* mutation cooperates with *Rb1* loss to confer an AR^{low}, ADT-resistant phenotype.

To test this hypothesis, we bred PBCre4:*Pten*$^{f/f}$: *Rb1*$^{f/f}$:*Trp53*$^{f/f}$ (TKO) mice. TKO mice developed aggressive prostate cancer, limiting median survival to 16 weeks (Fig. 2F). Metastasis to the lung, liver, and bone (one of four mice examined) was detected in TKO mice despite their short life span (fig. S5A). Castration of TKO mice at 10 weeks did not extend survival (Fig. 2G), demonstrating that TKO PADC was ADT-resistant de novo. Primary TKO tumors showed patchy Krt8 and Syp expression like DKO tumors but had very low AR levels comparable with that of postcastration recurrent DKO tumors (Fig. 2H). Surprisingly, pAKT levels were also reduced in TKO tumors despite uniform Pten loss (fig. S5B). Thus, TKO tumors have reduced dependence on both AKT and AR signaling. We also examined young PBCre4:*Pten*$^{f/f}$:*Rb1*$^{f/f}$:*Trp53*$^{f/+}$ mice retaining one wild-type copy of *Trp53*. In these mice, the appearance of Syp^{+} neoplastic cells occurred earlier than in DKO mice and was coincident with reduced levels of the Trp53 target gene *Cdkn1a* (fig. S5C). This suggests that spontaneous loss of the remaining wild-type *Trp53* allele facilitates the onset of Syp expression. These observations support the conclusion that *Rb1* and *Trp53* cooperate to suppress prostate cancer lineage plasticity underlying the development of ADT-resistant NEPC variants.

We next compared the gene expression patterns of SKO, DKO, and TKO tumors with that of normal prostate tissue. Gene expression patterns clustered primarily by genotype (fig. S6A). DKO and TKO tumors exhibited widespread changes in gene expression, encompassing ~15% of mouse genes (Fig. 3A). DKO and TKO tumors shared 85 to 90% of their differentially expressed genes. This similarity in gene expression between DKO and TKO tumors was not due to spontaneous silencing of *Trp53* expression in DKO tumors (fig. S6B).

This implies that the primary driver of gene expression reprogramming in DKO and TKO tumors is *Rb1* loss.

Consistent with immunostaining results, DKO and TKO tumors exhibited decreased levels of AR RNA and elevated levels of neuroendocrine lineage marker RNA (Figs. 1B and 2H and fig. S6C). These changes are similar to those observed in human NEPC variants. To compare prostate cancer in these mouse models with the human disease, we used a weighted gene expression signature developed by Beltran *et al.* (5, 23) to distinguish human adenocarcinoma from NEPC variants. We found that SKO cancer was similar to human PADC, whereas DKO and TKO cancers were similar to human NEPC (Fig. 3B). The Beltran signature accurately distinguishes SKO from DKO/TKO tumors through hierarchical clustering (fig. S6D).

Gene set enrichment analysis revealed that DKO and TKO tumors have altered expression of E2F target genes and neuroendocrine lineage genes (Fig. 3C). We also noted altered expression of gene sets related to stem cells and epigenetic reprogramming, including increased expression of *Sox2* [SRY (sex determining region Y)-box 2] and *Ezh2* (histone methyltransferase enhancer of zeste homolog 2) (Fig. 3, D to F). Gene expression changes corresponding to stem cell reprogramming factors and neuroendocrine lineage markers were associated with a switch in posttranslational histone H3 modifications from the repressive H3K27me3 mark to the active H3K4me3 mark (fig. S7). Human NEPC also exhibited increased expression of E2F target genes, neuroendocrine markers, stem cell reprogramming factors, and epigenetic regulators (Fig. 3G). Thus, DKO and TKO prostate cancers mimic the molecular phenotype of human NEPC variants, and both human and mouse NEPC variants exhibit deregulation of stem cell reprogramming factors.

Rb1/E2f protein complexes can directly repress expression of *Sox2* and *Ezh2* (24, 25). We hypothesized that *Rb1* loss in prostate cancer derepresses these genes, enabling epigenetic reprogramming toward a stem cell–like state. Lineage plasticity inherent in this state would facilitate metastasis, NEPC transformation, and ADT resistance. This hypothesis predicts that ADT resistance may be reversible through appropriate epigenetic modulation.

Ezh2 is the enzymatic component of the Polycomb Repressive complex 2 that methylates the lysine 27 residue of histone H3. Ezh2 inhibitors (Ezh2i) are being evaluated as cancer therapies in clinical trials. We isolated cell lines from mouse prostate cancers to test whether Ezh2i can restore ADT sensitivity in vitro. The cell lines behave like the tumors from which they were derived. For example, SKO, DKO, postcastration recurrent DKO (DKOCr), and TKO cell lines exhibit differences in AR expression, AR activity, neuroendocrine lineage marker expression, *Ezh2* and *Sox2* expression, cell proliferation, and motility analogous to the behavior of their corresponding tumors in vivo (fig. S8, A to G). Enzalutamide sensitivity was highest in SKO cells, reduced in DKO cells, and lowest in cells from postcastration recurrent DKO (DKOCr) and TKO tumors (fig. S8H).

We tested two Ezh2 inhibitors (Ezh2i), GSK126 and EPZ6438, and found that they both sensitized TKO and DKOCr cells to enzalutamide when used at concentrations sufficient to inhibit histone H3K27 methylation but without significant single-agent cell growth

inhibitory activity (Fig. 4, A to C, and fig. S9, A and B). Ezh2i plus enzalutamide also had a greater effect on DKO cells than either drug as single agents (fig. S9C), and Ezh2i pretreatment inhibited DKO cell motility (fig. S9E). Ezh2i did not significantly alter the enzalutamide sensitivity of SKO cells (fig. S9D), suggesting that its effects are specific for NEPC variants. We also evaluated the effects of Ezh2i in vivo. We propagated a primary DKOCr tumor by transplantation into SCID mice and then treated the mice with Ezh2i and enzalutamide, alone or in combination. Enzalutamide plus Ezh2i treatment slowed tumor growth significantly compared with treatment with enzalutamide [two-way analysis of variance (ANOVA) $P = 0.037$] or Ezh2i ($P = 0.027$) alone (Fig. 4D). Enzalutamide treatment alone did not slow tumor growth relative to vehicle control ($P = 0.43$), confirming that the DKOCr tumor was ADT-resistant.

To genetically verify Ezh2 as the relevant target of Ezh2i, we silenced *Ezh2* expression using short hairpin RNA (shRNA). *Ezh2* silencing sensitized DKOCr cells to enzalutamide (Fig. 4, E and F). Silencing *Ezh2* also increased AR expression, augmented AR activity, increased expression of the luminal lineage marker *Krt8*, and decreased expression of neuroendocrine lineage markers (Fig. 4, F and G). Ezh2i treatment also increased AR expression and decreased Syp expression in vitro (Fig. 4H). Ezh2i-treated transplanted DKOCr tumors showed evidence of increased AR expression in vivo (Fig. 4I), although immunostaining was patchy with both AR^{high} and AR^{low} regions present. These findings suggest that Ezh2i sensitizes NEPC variants to enzalutamide by reversing or suppressing lineage transformation.

To investigate whether Ezh2i has similar effects in human prostate cancer, we used LNCaP-AR cells from Mu *et al.* (26) in which *RB1* and *TP53* expression is stably silenced. Because LNCaP-AR cells were *PTEN*-null (27), *RB1*- and *RB1*/*TP53*–silenced derivatives were analogous to DKO and TKO mouse cells, respectively. As in mouse cells, *RB1* and *RB1*/*TP53* silencing reduced AR levels and enzalutamide sensitivity, but enzalutamide sensitivity was restored by Ezh2i (Fig. 4J and fig. S9F). Thus, enzalutamide resistance is reversible in both human and mouse NEPC variants.

Rb1 and *Trp53* repress epigenetic reprogramming factors such as Ezh2 and Sox2, which are important in generating induced pluripotent stem cells (24, 28, 29). The data presented here support a hypothesis in which *RB1* and *TP53* loss in prostate cancer derepresses these same factors, creating a stem cell–like epigenetic environment permissive for lineage plasticity (Fig. 4K). Lineage plasticity is proposed to drive prostate cancer progression by enabling adaptation to selective pressures experienced during metastasis and ADT. Because the mouse models characterized in this study develop metastatic PADC reminiscent of human NEPC variants, they will be useful for testing this hypothesis and identifying molecular mechanisms underlying cancer lineage plasticity. Our results also suggest a therapeutic approach to treat NEPC variants—that is, epigenetic modulation may reverse or delay lineage transformation, extending the durability of clinically beneficial ADT responses. As lineage plasticity is increasingly appreciated in other types of human cancers relapsing from molecularly targeted therapy, this approach may be generally applicable.

Supplementary Material

Refer to Web version on PubMed Central for supplementary material.

Acknowledgments

RNA-seq data generated in this study are deposited in the Gene Expression Omnibus (accession no. GSE90891). We acknowledge the RPCI writing group for critical reading of the manuscript and helpful comments. We thank H. Baumann for important assistance with multispectral imaging. The work was supported by funding from the National Cancer Institute (NCI) (grants R21 CA179907 and R01 CA70292 to D.W.G.; R01 CA155169, R01 CA19387, and P50 CA092629 to C.L.S.). P.M. was supported by a Congressionally Directed Medical Research Programs Prostate Cancer Research Program Postdoctoral Prostate Cancer Training Award (PC141607). L.E. and D.P.L. were supported by Prostate Cancer Foundation Young Investigator Awards. D.W.G. and M.S. were supported by the Roswell Park Alliance Foundation. D.P.L. is a recipient of a Scholarship for the Next Generation of Scientists from the Cancer Research Society and a Canadian Institute of Health Research Fellowship. C.L.S. was supported by the Howard Hughes Medical Institute (SU2C/AACR DT0712). The study was supported by the NCI RPCI Cancer Center Support Grant (P30 CA016056) and the NCI MSKCC Cancer Center Support Grant (P30 CA008748, P3 CA008748). C.L.S. is a co-inventor of enzalutamide and may be entitled to royalties. Enzalutamide is commercially available from Selleck Chemicals. C.L.S. serves on the board of directors of Novartis and is a paid consultant to ORIC Pharmaceuticals.

REFERENCES AND NOTES

1. Sequist LV, et al. Sci Transl Med. 2011; 3:75ra26.
2. Niederst MJ, et al. Nat Commun. 2015; 6:6377. [PubMed: 25758528]
3. Beltran H, et al. Clin Cancer Res. 2014; 20:2846–2850. [PubMed: 24727321]
4. Pezaro CJ, et al. Eur Urol. 2014; 65:270–273. [PubMed: 24295792]
5. Beltran H, et al. Nat Med. 2016; 22:298–305. [PubMed: 26855148]
6. Guo CC, et al. Hum Pathol. 2011; 42:11–17. [PubMed: 21040948]
7. Lotan TL, et al. Mod Pathol. 2011; 24:820–828. [PubMed: 21336263]
8. Williamson SR, et al. Mod Pathol. 2011; 24:1120–1127. [PubMed: 21499238]
9. Aparicio AM, et al. Clin Cancer Res. 2016; 22:1520–1530. [PubMed: 26546618]
10. Tan HL, et al. Clin Cancer Res. 2014; 20:890–903. [PubMed: 24323898]
11. Robinson D, et al. Cell. 2015; 161:1215–1228. [PubMed: 26000489]
12. Cancer Genome Atlas Research Network. Cell. 2015; 163:1011–1025. [PubMed: 26544944]
13. Wang S, et al. Cancer Cell. 2003; 4:209–221. [PubMed: 14522255]
14. Wu X, et al. Mech Dev. 2001; 101:61–69. [PubMed: 11231059]
15. Trotman LC, et al. PLOS Biol. 2003; 1:E59. [PubMed: 14691534]
16. Ding Z, et al. Nature. 2011; 470:269–273. [PubMed: 21289624]
17. Chen Z, et al. Nature. 2005; 436:725–730. [PubMed: 16079851]
18. Zhou Z, et al. Cancer Res. 2006; 66:7889–7898. [PubMed: 16912162]
19. Maddison LA, Sutherland BW, Barrios RJ, Greenberg NM. Cancer Res. 2004; 64:6018–6025. [PubMed: 15342382]
20. Muzumdar MD, Tasic B, Miyamichi K, Li L, Luo L. Genesis. 2007; 45:593–605. [PubMed: 17868096]
21. Livet J, et al. Nature. 2007; 450:56–62. [PubMed: 17972876]
22. Zhou Z, Flesken-Nikitin A, Nikitin AY. Cancer Res. 2007; 67:5683–5690. [PubMed: 17553900]
23. Beltran H, et al. Cancer Discov. 2011; 1:487–495. [PubMed: 22389870]
24. Kareta MS, et al. Cell Stem Cell. 2015; 16:39–50. [PubMed: 25467916]
25. Bohrer LR, Chen S, Hallstrom TC, Huang H. Endocrinology. 2010; 151:5136–5145. [PubMed: 20881251]
26. Mu P, et al. Science. 2017; 355:84–88. [PubMed: 28059768]
27. Li J, et al. Science. 1997; 275:1943–1947. [PubMed: 9072974]

28. Bracken AP, et al. EMBO J. 2003; 22:5323–5335. [PubMed: 14532106]
29. Hong H, et al. Nature. 2009; 460:1132–1135. [PubMed: 19668191]

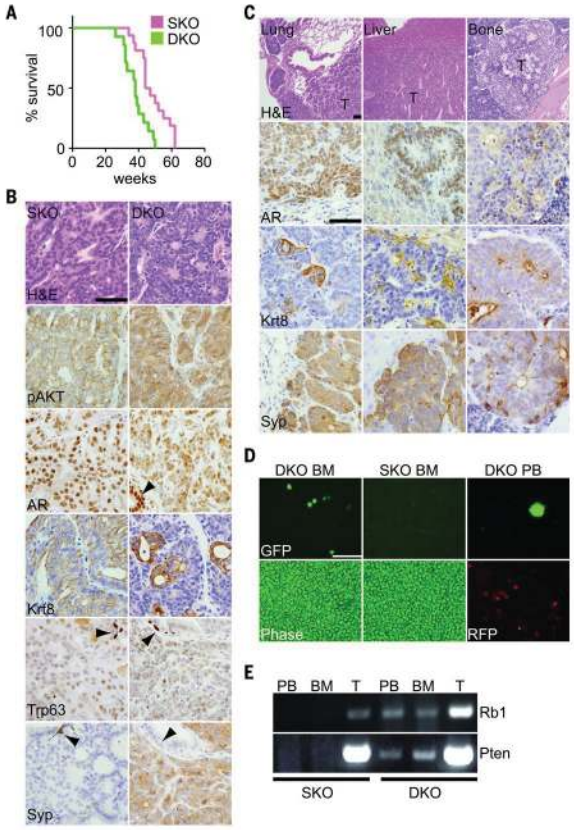

Fig. 1. *Rb1* suppresses PADC metastasis in mice

(**A**) Survival plot showing a significant difference in survival of SKO ($n = 16$) and DKO ($n = 14$) mice (log rank $P = 0.0013$). (**B**) End-stage tumor sections stained with hematoxylin and eosin (H&E) or antibodies against the indicated proteins. Arrowheads indicate uninvolved prostate epithelium. Scale bars, 100 μm. (**C**) Sections of DKO metastases from indicated tissues stained and presented as in (B). (**D**) Bone marrow (BM) or peripheral blood (PB) from SKO and DKO mice was imaged under phase or fluorescent microscopy. Cancer cells were genetically marked with green fluorescent protein (GFP), and normal cells were marked with red fluorescent protein (RFP). Scale bar, 100 μm. (**E**) Polymerase chain reaction (PCR) was used to detect Cre-deleted alleles in PB, BM, or tumor DNA (T).

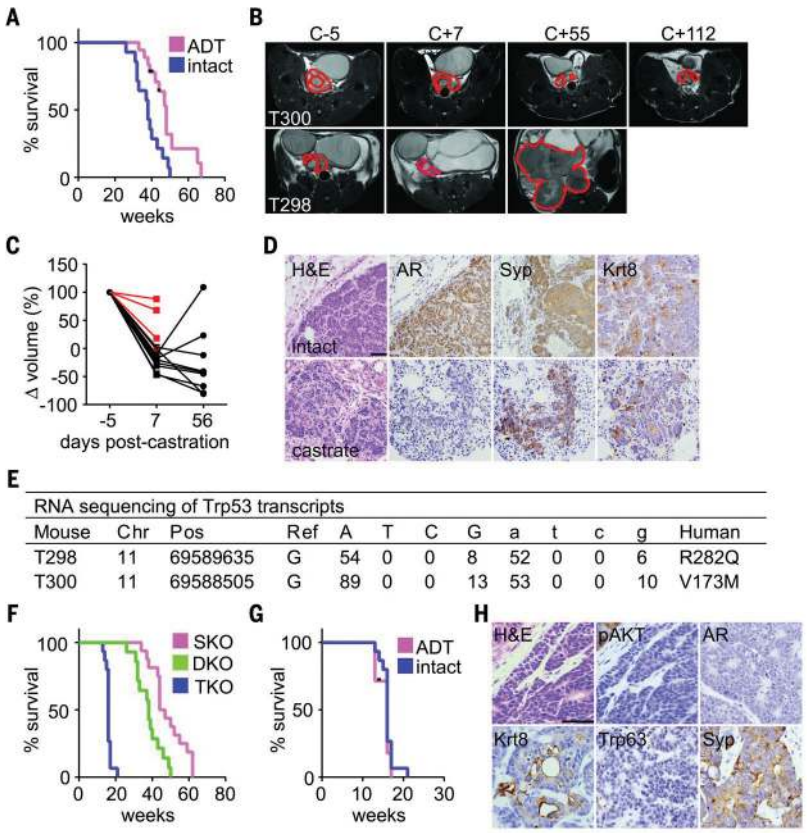

Fig. 2. *Rb1* and *Trp53* loss facilitate acquisition of ADT resistance

(**A**) Survival plot for DKO mice, either intact ($n = 14$) or castrated at 30 weeks ($n = 18$, log rank $P = 0.003$). Black tic marks represent mice alive at the end of the study. (**B**) Axial T2-weighted MR images from two mice acquired at indicated times relative to castration. The prostate and resulting tumors are outlined in red. T300 initial prostate volume (68 mm^3) was larger than T298 (21 mm^3), but T300 survived longer after castration (37 weeks) than did T298 (12 weeks). (**C**) Prostate volumes of DKO mice were measured with magnetic resonance imaging (MRI) 5 days before castration at 30 weeks of age, or 1 and 8 weeks after castration. The plot shows relative prostate volumes for individual mice over time normalized to their precastration measurement. Red lines indicate mice that died before the 8-week MRI time point. (**D**) Tumor sections from intact or postcastration recurrent DKO tumors stained with H&E or antibodies directed against the indicated proteins. AR levels decline in postcastration recurrent tumors. Scale bar, 100 μm. (**E**) RNA-seq data from postcastration recurrent DKO tumors indicate that 88% of reads mapping to *Trp53* have mutations analogous to loss-of-function mutations commonly found in human cancer. Single-letter abbreviations for the amino acid residues are as follows: A, Ala; C, Cys; D, Asp; E, Glu; F, Phe; G, Gly; H, His; I, Ile; K, Lys; L, Leu; M, Met; N, Asn; P, Pro; Q, Gln; R, Arg; S, Ser; T, Thr; V, Val; W, Trp; and Y, Tyr. In the mutants, other amino acids were substituted at certain locations; for example, R282Q indicates that arginine at position 282 was replaced by glutamine. (**F**) Survival plot showing significantly different survival of SKO ($n = 16$), DKO ($n = 14$), and TKO ($n = 15$) mice (log rank $P < 0.0001$). (**G**) Survival plot of TKO mice, either intact ($n = 15$) or castrated at 10 weeks ($n = 7$). Castration does not affect

survival significantly (log rank $P = 0.46$). Black tic marks represent mice alive at the end of the study. (**H**) Tumor sections from TKO mice were stained with H&E or antibodies against the indicated proteins. Scale bar, 100 μm.

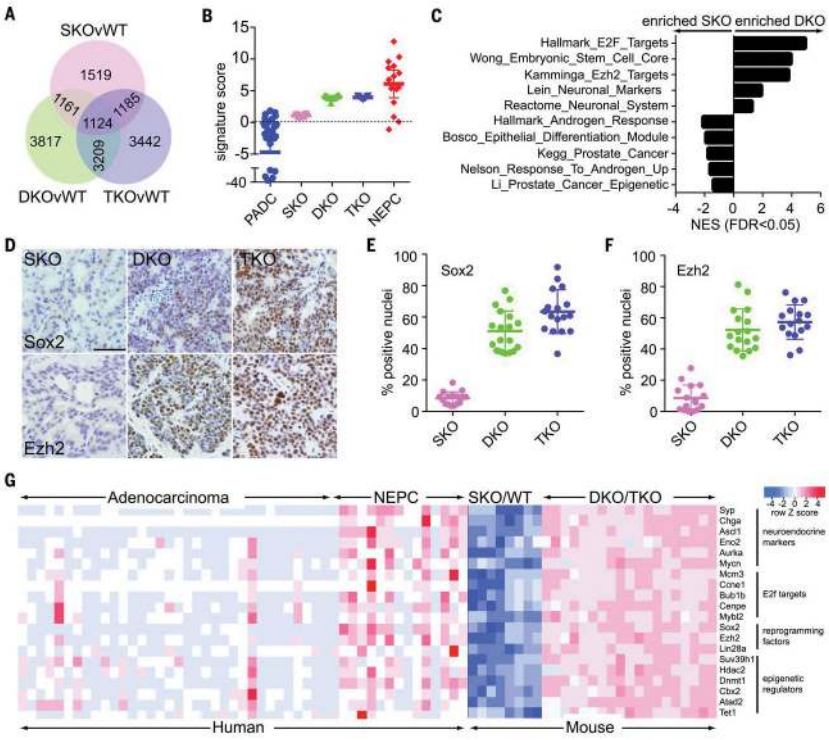

Fig. 3. *Rb1* loss causes deregulation of epigenetic reprogramming factors and widespread changes in gene expression

(**A**) Venn diagrams showing the number of differentially expressed genes between the indicated genotypes (wild type, WT; $n = 4$ or 5 mice per genotype). (**B**) Plot showing the signature scores for mouse (SKO, DKO, and TKO) and human (PADC and NEPC) prostate cancer by using the Beltran *et al.* (23) weighted gene expression signature. Dots represent individual patients. Bars represent the mean and interquartile range. (**C**) Selected gene sets enriched in DKO versus SKO tumors, with the *x* axis representing normalized enrichment score (NES). (**D**) Tumor sections stained with antibodies directed against indicated proteins. Scale bar, 100 μm. (**E**) Quantitation of Sox2 immunostaining in tumor sections of the indicated genotypes. Each dot represents one analyzed image taken from three different mice for each genotype, with bars representing the mean and standard deviation. Sox2 immunostaining in DKO tumors is greater than in SKO tumors (*t* test $P < 0.0001$) and greater in TKO tumors than in DKO tumors ($P = 0.01$). (**F**) Quantitation of Ezh2 immunostaining as in (E). Ezh2 immunostaining is greater in DKO tumors than in SKO tumors ($P < 0.0001$), but immunostaining in DKO and TKO tumors is not significantly different ($P = 0.25$). (**G**) A heat map comparing gene expression data from human (5, 23) and the indicated mouse specimens. The select genes deregulated in DKO and TKO tumors are similarly deregulated in human NEPC.

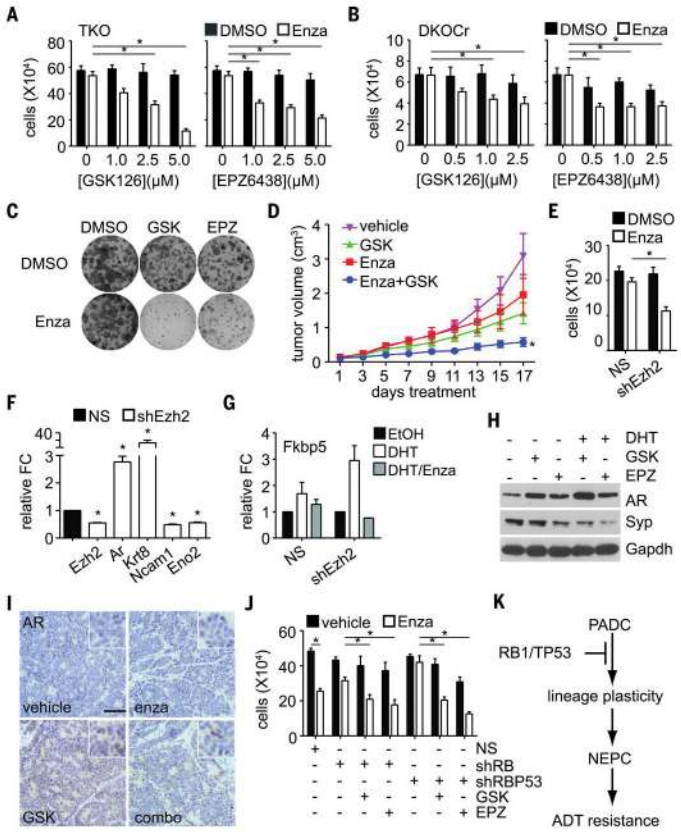

Fig. 4. Ezh2 inhibition restores enzalutamide sensitivity

(**A**) A TKO cell line was treated with enzalutamide or dimethyl sulfoxide (DMSO), with or without Ezh2i, at the indicated concentrations, and the viable cells were then counted. Mean cell number and standard error are shown for three experiments. Asterisks indicate significant differences ($P < 0.05$). (**B**) A DKOCr cell line was treated and analyzed as in (A). (**C**) A DKOCr cell line was plated at low density, then treated as indicated. Resulting colonies were stained 10 days later. A representative result is shown (quantitation is provided in fig. S8A). (**D**) A DKOCr tumor was transplanted into a cohort of mice, and the mice were treated with GSK503 (GSK) and/or enzalutamide (Enza) as indicated. Tumor volume for each mouse ($n = 7$ or 8 for each treatment) was recorded every other day. The mean and standard error for all mice are shown. Asterisk indicates significantly slower growth than any of the other treatments (ANOVA, $P < 0.05$). (**E**) *Ezh2*-targeted shRNA (shEzh2), or nonsilencing control (NS), were expressed in DKOCr cells. The cells were then treated with enzalutamide or DMSO, and cell number was measured as in (A). The mean and standard error for three experiments are shown. (**F**) RNA was extracted from DKOCr cells in (E) and analyzed by means of real-time PCR for the indicated genes. The mean and standard error of fold change (FC) relative to the NS control are shown for two experiments in duplicate. (**G**) DKOCr cells silenced for *Ezh2* as in (C) were treated with AR ligand R1881 (DHT) and/or enzalutamide (Enza), RNA was extracted, and the expression of AR target gene *Fkbp5* was assayed by means of real-time PCR. Mean and standard error of FC relative to the NS control are shown for two experiments in duplicate. (**H**) DKO cells were treated as indicated, and protein extracts were analyzed by means of Western blot for the

listed proteins. Gapdh serves as loading control. (**I**) Tumors dissected from transplanted mice in (D) after 17 days of the indicated treatment were sectioned and immunostained for AR. Inset image is magnified so as to highlight nuclear staining. Scale bar, 100 μm. Ezh2i treatment restores patchy AR expression. (**J**) LNCaP-AR cells stably expressing *RB1* (shRB) or *RB1*/*TP53* shRNA (shRBP53) were treated as indicated, and viable cells were counted as in (A). The mean and standard error of three experiments are shown. (**K**) A model summarizing the proposed role of *Rb1* and Trp53 in suppressing lineage plasticity, neuroendocrine lineage transformation, and ADT resistance.